Nonlocal correlations in a proximity-coupled normal metal

Taewan Noh[1], Sam Davis[2], and Venkat Chandrasekhar[1,2]
[1]*Department of Physics and Astronomy, Northwestern University, Evanston, IL 60208, USA,*
[2]*Graduate Program in Applied Physics, Northwestern University, Evanston, IL 60208, USA*
(Dated: November 1, 2012)

We report evidence of large, nonlocal correlations between two spatially separated normal metals in superconductor/normal-metal (SN) heterostructures, which manifest themselves a nonlocal voltage generated in response to a driving current. Unlike prior experiments in SN heterostructures, the nonlocal correlations are mediated not by a superconductor, but by a proximity-coupled normal metal. The nonlocal correlations extend over relatively long length scales in comparison to the superconduncting case. At very low temperatures, we find a reduction in the nonlocal voltage for small applied currents that cannot be explained by the quasiclassical theory of superconductivity. We believe is a signature of new long-range quantum correlations in the system.

PACS numbers: 74.45+c, 03.67.Mn, 74.78.Na

Electrons in spatially separated normal metals in mutual contact with a superconductor show correlations that are evidence of quantum entanglement due to their interaction with the Cooper pairs in the superconductor. [1–8] Experimentally, the correlations manifest themselves as a nonlocal voltage that develops on one normal metal in response to a current injected from another normal metal into the superconductor. In such a hybrid structure, three processes that contribute to the nonlocal voltage have been investigated. Two, crossed Andreev reflection (CAR) and elastic co-tunneling (EC), arise from the interaction of quasiparticles in the spatially separated normal metals that are mediated by the Cooper pairs in the superconductor, and decay spatially on the scale of the superconducting coherence length ξ_S, typically $\sim$ 100 nm for Al [4, 6]. The third process, charge imbalance [9, 10], is associated with the conversion of a quasiparticle current into a supercurrent in the superconductor, and decays over the charge imbalance length Λ_{Q^*}, which is of the order of a few microns [11–13]. None of these three nonlocal processes are expected in a normal metal with an induced superconducting proximity effect, where there is no superconducting order parameter. Consequently, it comes as a surprise that large nonlocal signals can indeed be observed when a quasiparticle current is injected into a normal metal that is proximity coupled to two superconductors. The experimental manifestation of these nonlocal signals is very similar to that observed in NSN structures [11–18], although their origin appears to be quite different.

The samples measured in this work had Au as the normal metal and Al as the superconductor. The length L of the normal wire between the two superconducting films was designed such that the two superconductors were Josephson-coupled in the temperature range of interest. For diffusive conductors, this occurs at temperatures below $\sim E_c/k_B$, where $E_c = \hbar D/L^2$ is the Thouless energy and D the electronic diffusion coefficient. The temperature dependence of Josephson coupling is determined by the Thouless length $L_T = \sqrt{\hbar D/k_B T}$, where T is the temperature. For this sample, which had D=110 cm^2/s so that $E_c = 11.7$ μeV and $L_T = 293$ nm$/\sqrt{T}$, a finite supercurrent was observed below $\sim$0.7 K. Given the multiprobe nature of the sample, we shall use the notation $R_{ij,kl} = dV_{kl}/dI_{ij}$ to denote the four-terminal differential resistance, where the ac and dc current is applied between contacts i and j, and the resulting ac voltage measured between contacts k and l, with the contacts numbered as in Fig. 1a.

Figure 1b shows a measurement of the local differential resistance $R_{19,28}$ as a function of I_{dc} at T=20 mK. The position of the peaks in this curve identify the critical current I_c. The blue circles in Fig. 1c show the T dependence of I_c, and the solid line is a fit to the functional form $I_c = BT^{3/2}\exp(-A/L_T)$ (where A and B are constants) expected for a SNS junction in the long junction limit [19] ($\Delta >> E_c$, where Δ is the gap in the superconductor). As can be seen, the fit is quite good. I_c at base temperature is smaller than the value $I_{c0} = 10.82E_c/eR_N$ predicted for a simple SNS junction[19] (R_N is the normal state resistance). For this sample, $I_{c0}eR_N/E_c \sim 0.56$, with $R_N = 4.56$ Ω. However, in multiterminal structures I_c is suppressed [20] due to a modification of the induced minigap. If we assume that the measured I_{c0} is related to an effective Thouless energy E_c^* by the same theoretical prediction for a simple SNS junction, we obtain $E_c^* = 0.59$ μeV.

We now discuss the nonlocal measurements. Figure 2a shows the nonlocal dV/dI at 20 mK for four different configurations, each with the current sourced through normal electrode 3 and drained through a superconducting electrode 1. The overall shape of the resulting traces is remarkably similar to what is observed in previous measurements on NSN devices [16, 17]: at $I_{dc} = 0$, dV/dI is finite and grows with current, resulting in a peak at a finite current of $\sim$ 2.3 μA, after which there is a sharp drop to negative values before it goes to zero at high bias. In the case of NSN structures, a similar peak followed by

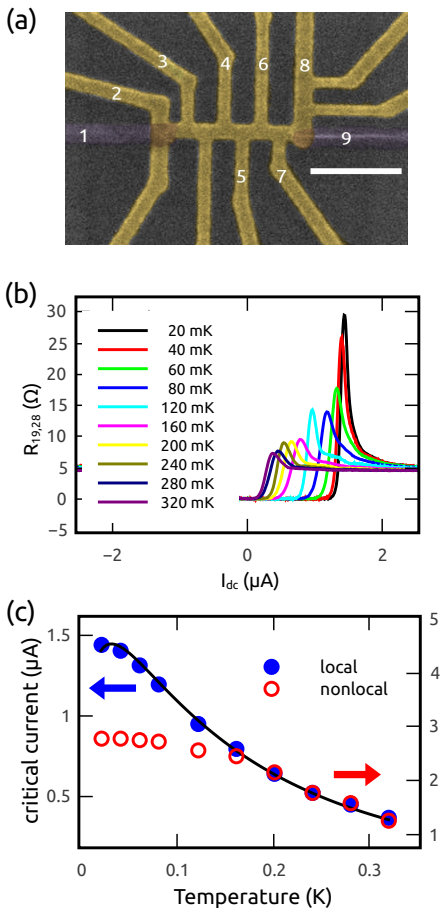

FIG. 1: (a) False color scanning electron micrograph of the sample discussed in the text. Light areas are Au; the darker lines are Al. The numbers mark the contacts used for four-terminal differential resistance measurements. The size bar is 500 nm. (b) Local differential resistance $R_{19,28}$ as a function of the applied current I_{dc}, showing the critical current of the SNS junction. (c) Blue circles show the measured critical current, determined by the position of the peak in the differential resistance in (b), as a function of temperature T. The solid line shows a fit to the expected temperature dependence for a long SNS junction of length L [19]. Open red circles are the finite values of I_{dc} at which the nonlocal differential resistance $R_{31,49}$ (Fig. 2(a)) has its minimum.

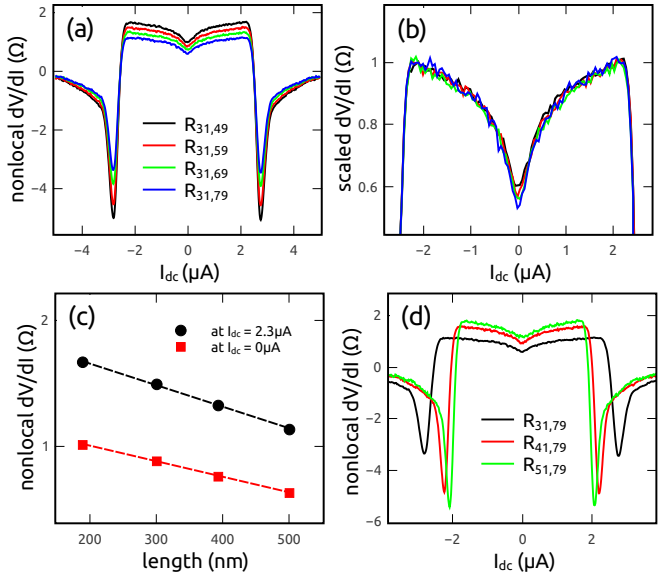

FIG. 2: (a) Nonlocal resistances as a function of dc current bias for 4 nonlocal configurations, $R_{31,49}$, $R_{31,59}$, $R_{31,69}$ and $R_{31,79}$. (b) Data of (a), with the curves for $R_{31,49}$, $R_{31,59}$, $R_{31,69}$ and $R_{31,79}$ scaled so that their normalized peaks at ± 2.3 μA match. (c) Nonlocal resistance at 2.3 μA (black symbols) and at zero bias (red symbols), taken from (a), as a function of the distance between the respective voltage contact and the current injection point. The straight lines are linear fits to the data. (d) Nonlocal resistances $R_{31,79}$, $R_{41,79}$ and $R_{51,79}$, where the current injection terminal is changed, but the voltage contacts remain the same.

a dip was associated with I_{dc} exceeding I_c of the superconductor. Here, as discussed below, this feature results from *part* of I_{dc} exceeding I_c of the SNS junction [16, 21]. dV/dI also decreases as the distance of the normal voltage contact from the current injection node increases. While the overall shape of the traces is similar to that observed nonlocal NSN devices, there are some significant differences. In particular, there is a sharp dip in dV/dI near $I_{dc} = 0$ that is not present in nonlocal NSN measurements.

In the nonlocal NSN experiments [16, 17], it was found that the zero bias differential resistance $R_{nl}(0)$ and the peak at finite I_{dc} decayed with the distance from the current injection electrode, but with different length scales: while the zero bias resistance decayed exponentially with ξ_S as expected from CAR/EC, the peak was associated with charge imbalance and found to decay linearly with Λ_{Q^*}. In the current experiments, $R_{nl}(0)$ and the peak resistance also scale differently with distance. Figure 2b shows the curves of Fig. 2a scaled so that their peaks at finite bias match. With this scaling, the curves match over most of the range of current, except near zero bias. This shows clearly that $R_{nl}(0)$ and the finite bias resistance scale differently with length, as was found for the NSN samples. In the NSN case, $R_{nl}(0)$ decayed exponentially on a length scale of ξ_S: Here one might expect that $R_{nl}(0)$ should decay exponentially with L_T. Figure 2c shows that, contrary to expectation, both $R_{nl}(0)$ and the peak resistance show an almost perfect linear dependence on the distance from the current injection point, although the slopes are different, reflecting the different scaling evident in Fig. 2b.

What is the origin of this behavior? In NS structures with Josephson coupling between two superconducting electrodes, supercurrents and quasiparticle currents can coexist in a proximity-coupled normal metal over distances much longer than ξ_S [22–24]. As the superconducting electrodes S_1 and S_2 are Josephson-coupled at

low enough temperatures, they are at the same electrochemical potential, which we take to be 0 here for simplicity. A finite potential V applied to the current injection electrode N_1 will drive a quasiparticle current I_{qp} into the proximity-coupled normal metal (Fig. 3a). Since S_1 and S_2 are both at zero potential, this quasiparticle current will split into two components: I_{qp1} will flow towards S_1, and I_{qp2} will flow towards S_2, the ratio I_{qp1}/I_{qp2} being determined by the inverse ratio of the resistances of the normal sections between the current injection point and $S_{1,2}$. As S_2 is a voltage probe, no net current can flow into it. Hence I_{qp2} must be balanced by a counterflowing supercurrent I_S that flows from S_2 to S_1 such that $I_S = -I_{qp2}$ and $I_S + I_{qp1} = I_{qp}$, in turn giving rise to a phase difference ϕ between S_1 and S_2. This situation will persist until I_S exceeds I_c of the junction. Since I_{qp1} is always less than I_{qp}, the injected dc current I_{qp} at which this occurs is always greater than I_c. Evidence for this model can be seen by examining the value of current at which this occurs. The red open circles in Fig. 1c show the value of I_{dc} as a function of T at which the minimum in the resistance at finite bias is observed in the nonlocal measurement (Fig. 2a). The ordinate axis has been scaled so that the data points lie on top of the measured I_c (blue circles) at high temperatures. At lower temperatures, however, they show a weaker temperature dependence. This latter behavior has been observed previously by other groups [24], and arises from the reduction of I_c due to the nonequilibrium quasiparticle distribution introduced by I_{qp} [22].

I_{qp2} will result in a finite "nonlocal" voltage between the normal voltage contacts $N_{2,3}$ and the second superconductor S_2 that will be proportional the resistance of the normal wire between $N_{2,3}$ and S_2, plus the resistance of the interface NS_2. Thus, one would expect to see the linear scaling shown in Fig. 2c. In addition, as the current injection point is moved closer to S_2, one would expect to see an increase in the nonlocal voltage (and hence differential resistance) as the ratio I_{qp2}/I_{qp} increases. Figure 2d, which shows the nonlocal differential resistance for a fixed voltage lead but different current injection points, confirms this.

Hence it appears that the current separation model describes well the nonlocal resistance that we observe. However, closer analysis of the current bias and temperature dependence of the nonlocal resistance reveals some significant discrepancies. Quantitative predictions for the differential resistance can be obtained by simultaneously solving numerically the Usadel equations as well as the kinetic equations for the nonequilibrium distribution functions [26] to obtain the nonlocal dV_{nl}/dI_{qp} as a function of I_{qp}, and $R_{nl}(0)$ as a function of temperature. The resulting curves are shown in Figs. 3b and 3c respectively. (Details of the calculations are given in the Supplementary Information.) There are many differences between the results of the simulations and our measurements, but we shall focus here on the most significant discrepancy. Figure 3c shows that $R_{nl}(0)$ is expected to increase as T decreases. This behavior is simply the well-known reentrance effect of a proximity-coupled normal metal [27]: as the temperature is decreased below the transition temperature of the superconductor, the resistance of the normal metal first decreases, but then reaches a minimum at a certain temperature T_0, increas-

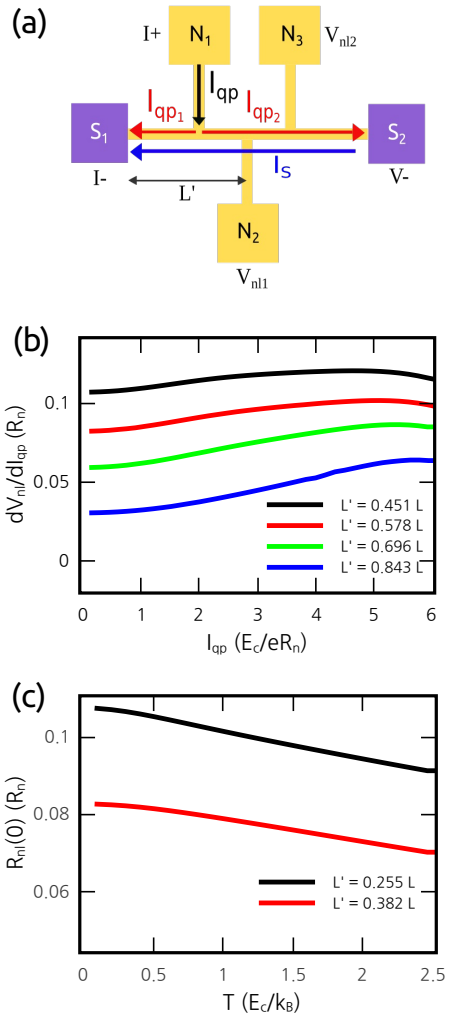

FIG. 3: (a) Schematic of the current separation model. The injected quasiparticle current I_{qp} splits into two currents, I_{qp1} and I_{qp2}, which go towards the two superconducting contacts S_1 and S_2 respectively. I_{qp2} is compensated by a counterflowing supercurrent I_s that flows from S_2 to S_1. (b) Results of the numerical simulations based on the quasiclassical theory of superconductivity for the nonlocal resistances for the geometry of (a) as a function of I_{qp}. The distance L' between the normal probe (on the normal metal) and S_1 is $0.451L$, $0.578L$, $0.696L$ and $0.843L$, where L is the length of normal metal between S_1 and S_2. The position of N_1 is fixed at $0.196L$ from S_1. These values are chosen to match the sample geometry. (c) Calculated zero bias resistance as a function of temperature. Details of the simulation are described in the Supplementary Information.

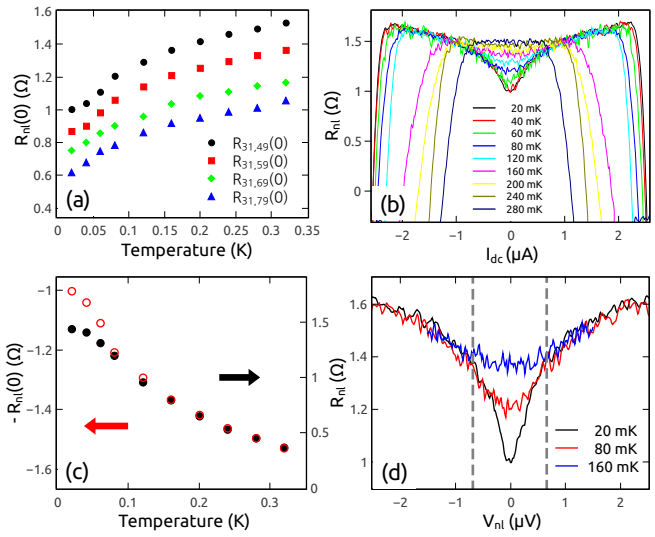

FIG. 4: (a) Temperature dependence of $R_{nl}(0)$ for all four nonlocal resistance configurations. (b) Nonlocal differential resistance for the closest configuration at a number of different temperatures. (c) Temperature dependence of $-R_{nl}(0)$ for the configuration in (b) and temperature dependence of the local critical current I_c. (d) Data from (b) at 20 mK, 80 mK and 160 mK, plotted as a function of the nonlocal voltage V_{nl} obtained by numerical integration. Dotted lines are guides to the eyes for the points where 20 mK and 80 mK data deviate significantly from 160 mK data.

ing as the temperature is decreased further. For a single N wire connected to a S reservoir, $T_0 \sim 5E_c/k_B$ [28]. For more complicated geometries, T_0 may be modified, and a self-consistent calculation as we have done is required. These calculations show that experimentally we are in the regime $T < T_0$, with the resistance rising as the temperature is decreased, since $L_T \geq L$ in the temperature regime of interest. The experimental data, however, show exactly the opposite trend. Figure 4a shows $R_{nl}(0)$ for the 4 nonlocal configurations of Fig. 2a in the low temperature regime. The nonlocal resistance *decreases* with decreasing temperature, in direct contrast to the behavior expected from Fig. 3c. At higher temperatures, the nonlocal resistance drops sharply to zero, which is due to the vanishing of the supercurrent between the superconducting electrodes, without which no nonlocal signal can be observed.

A clue to the origin of the decrease in $R_{nl}(0)$ with decreasing T can be seen in the temperature evolution of dV/dI vs. I_{dc}, which is shown in Fig. 4b for one nonlocal configuration. Apart from the decrease in I_c with increasing T, the only major difference between the different temperature traces is the growth of the dip at zero bias. In order to study the temperature dependence of this feature, we plot $-R_{nl}(0)$ together with the measured I_c of the SNS junction, with appropriate offset and scaling so that the data points coincide at higher temperatures. $-R_{nl}(0)$ matches the exponential behavior of I_c at higher temperatures, but the two curves diverge at lower temperatures, with I_c saturating, but $-R_{nl}(0)$ still showing a strong exponential dependence. To investigate the energy scales involved, we integrate the nonlocal differential resistance to obtain dV/dI vs V_{nl}. Figure 4c shows the 20, 80 and 160 mK from Fig. 4b plotted in this manner. The voltage at which the 20 mK curve deviates significantly from the 80 and 160 mK curves at low bias– the voltage at which the zero bias dip starts developing – is approximately 0.6 μV, much smaller than E_c/e, but in very good agreement with the effective Thouless energy E_c^*/e defined earlier. For nonlocal measurements on conventional NSN devices near zero bias, CAR is expected to give a negative contribution to the nonlocal resistance [2], as two electrons with energies less than Δ, one from each normal metal, combine to form a Cooper pair. The decrease in the nonlocal resistance in our samples suggests a similar process is happening in these samples, since the pair coupling in the proximity coupled normal metal is finite. Thus, two electrons, one from each normal lead, combine to form a correlated pair in the proximity coupled normal metal. Exactly how this process occurs is not clear, as it is not described by our current understanding of nonequilibrium transport in proximity-coupled normal metals.

In summary, measurements on proximity-coupled normal metals reveal a signature of long-range nonlocal quasiparticle correlations that may be related to the formation of pair correlations in the proximity-coupled normal metal. Further study is required to elucidate the origin of these correlations.

We thank P. Virtanen for help with his quasiclassical superconductivity numerical code. We also thank J. Koch for a careful reading of the manuscript. This research was supported by the NSF under grant No. DMR-1006445.

[1] J. M. Byers and M. E. Flatté, Phys. Rev. Lett. **74**, 306 (1995).
[2] G. Deutscher and D. Feinberg Appl. Phys. Lett. **76**, 487 (2000).
[3] G. Falci, D. Feinberg and F. W. J. Hekking Europhys. Lett. **54**, 255 (2001).
[4] D.Feinberg Euro. Phys. J. B **36**, 419 (2003).
[5] R. Mélin and D. Feinberg Phys. Rev. B **70**, 174509 (2004).
[6] A. Brinkman and A. A. Golubov Phys. Rev. B **74**, 214512 (2006).
[7] J. P. Morten, A. Brataas and W. Belzig Applied Physics A **89**, 609 (2007).
[8] A. L. Levy Yeyati, F. S. Bergeret, A. Martín-Rodero and T. M. Klapwijk Nature Physics **3**, 455 (2007).
[9] J. Clarke Phys. Rev. Lett. **28**, 1363 (1972).
[10] M. Tinkham and J. Clarke Phys. Rev. Lett. **28**, 1366 (1972).

[11] J. Brauer, F. Hübler, M. Smetanin, D. Beckmann and H. v. Löhneysen Phys. Rev. B **81**, 024515 (2010).
[12] F. Hübler, J. Camirand Lemyre, D. Beckmann and H. v. Löhneysen Phys. Rev. B **81**, 184524 (2010).
[13] K. Yu. Arutyunov, H. -P. Auraneva and A. S. Vasenko Phys. Rev. B **83**, 104509 (2011).
[14] D. Beckmann, H. B. Weber and H. v. LöhneysenPhys. Rev. Lett. **93**, 197003 (2004).
[15] S. Russo, M. Kroug, T. M. Klapwijk and A. F. Morpurgo Phys. Rev. Lett. **95**, 027002 (2005).
[16] P. Cadden-Zimansky and V. Chandrasekhar Phys. Rev. Lett. **97**, 237003 (2006).
[17] P. Cadden-Zimansky, Z. Jiang and V. Chandrasekhar New J. Phys **9**, 116 (2007).
[18] P. Cadden-Zimansky, J. Wei, V. Chandrasekhar Nat. Phys. **5**, 393 (2009).
[19] P. Dubos, H. Courtois, B. Pannetier, F. K. Wilhelm, A. D. Zaikin and G. Schön Phys. Rev. B **63**, 064502 (2001)
[20] P. Virtanen PhD Thesis, Helsinki University of Technology (2009)
[21] F. S. Bergeret, A. L. Yeyati Phys. Rev. B. **80**, 174508 (2009)
[22] J. J. A. Baselmans, A. F. Morpurgo, B. J. van Wees and T. M. Klapwijk Nature **397**, 43 (1999).
[23] R. Shaikhaidarov, A. F. Volkov, H. Takayanagi, V. T. Petrashov, and P. Delsing Phys. Rev. B **62**, (R)14649 (2000).
[24] M. S. Crosser, J. Huang, F. Pierre, P. Virtanen, T. T. Heikkilä, F. K. Wilhelm and N. O. Birge Phys. Rev. B **77**, 014528 (2008).
[25] C. J. Lambert and R. Raimondi J. Phys.: Condens. Matter **10**, 901 (1998)
[26] W. Belzig, F. K. Wilhelm, C. Bruder, G. Schön and A. D. Zaikin Superlattices Microstruct **25**, 1251 (1999)
[27] H. Courtois, Ph. Gandit, D. Mailly and B. Phys. Rev. Lett. **76**, 130 (1996)
[28] V. Chandrasekhar Physics of Superconductors, vol II, eds. Bennemann and Ketterson, Springer-Verlag, (2004)

Supplementary Information:

Nonlocal correlations in a proximity-coupled normal metal

T. Noh, S. Davis and V. Chandrasekhar

Department of Physics and Astronomy,

Northwestern University, Evanston, IL 60208

PACS numbers:

I. NONLOCAL MEASUREMENTS ON A NSN STRUCTURE AND CONTROL SAMPLES

Figure S1a shows an image of another sample that was measured. The length L of the normal wire between the two superconductors is shorter than that of the sample discussed in the main text. This sample had additional leads to perform control measurements. Figure S1b shows a nonlocal resistance measurement corresponding to earlier measurements on NSN structures.[1] (the numbers refer to the contacts numbered in Fig. S1a, with the same convention to specify the four terminal resistance as in the main text). It can be seen that the shape of the curve is very similar to what was observed previously. In particular, as shown in the inset, there is no sharp dip in the nonlocal resistance near zero bias. To emphasize the difference between this measurement in the NSN configuration and the nonlocal measurements on proximity-coupled normal metals, Fig. S1c shows the nonlocal resistance similar to Fig. 2 in the main text for the sample of Fig. S1a. A very pronounced dip is seen at zero bias.

To demonstrate that the nonlocal resistance is observed only when there is a supercurrent between the two superconducting contacts, we show nonlocal resistance measurements on another sample that is nominally identical to the sample of Fig 1 of the main text, except that it does not have a second superconducting contact (Fig. S2a). It can be seen that the nonlocal resistance is zero, showing that the presence of two superconductors is required to see the effect.

II. TEMPERATURE DEPENDENCE OF THE ZERO BIAS NONLOCAL RESISTANCE

Figure S3 shows the temperature dependence of the three different zero bias nonlocal resistances of the sample of Fig. 1 in the main text. It should be noted that while this cooling temperature sweep was performed over 5 hours, there is still some lag between the temperature read by the mixing chamber thermometer and the actual temperature of the sample, in contrast to the data shown in Fig. 2a of the main paper. Nevertheless, these data show that the nonlocal resistance is essentially zero above 0.8 K and increases rapidly below this temperature. This increase is associated with the establishment of Josephson coupling

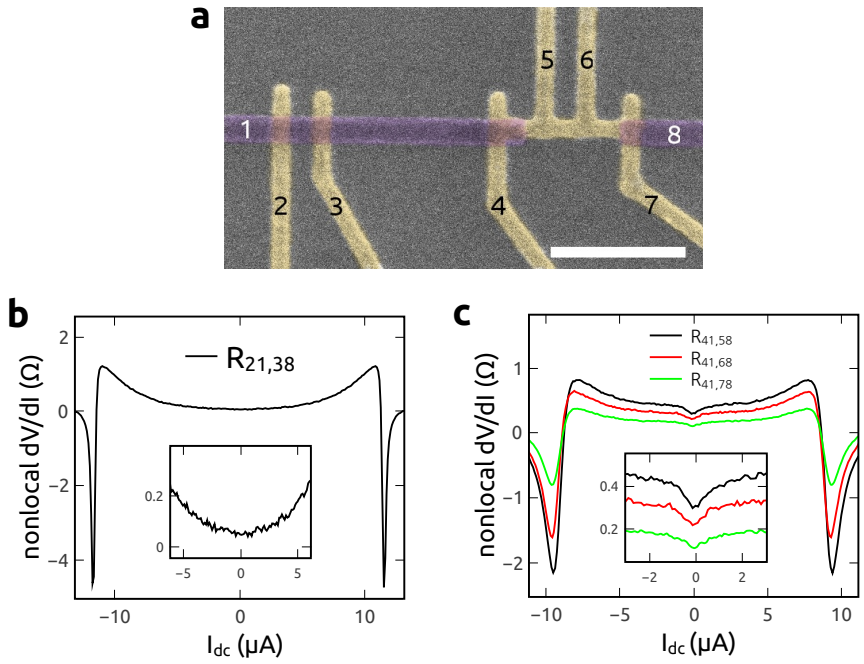

FIG. 1: **(a)** Scanning electron micrograph of another nonlocal sample, with terminals numbered as in the main text. The light areas are gold, the darker lines are Al. Size bar is 500 nm. **(b)** Nonlocal resistance measurement of the NSN configuration on the left, corresponding to previous measurements on NSN samples.[1] The numbers refer to contacts used for current and voltage leads, as described in the main text. Inset: Expanded view of the zero bias region, showing that there is no dip in nonlocal resistance near zero bias. **(c)** Nonlocal resistance of the proximity-coupled normal metal for the sample of **(a)**. Inset: Expanded view of the zero bias region, showing that there are pronounced dips in nonlocal resistances near zero bias.

between the two superconductors, as discussed in the main text. The decrease in resistance at lower temperatures is consistent with the development of the dip in nonlocal resistance seen in the nonlocal dV/dI at low temperatures (Fig. 4 in the main text).

III. NUMERICAL SIMULATIONS BASED ON THE QUASICLASSICAL THEORY OF SUPERCONDUCTIVITY

The numerical simulations in this paper were based on the Usadel equations of the quasiclassical theory of superconductivity, using the Riccati parametrization. We used the public domain numerical solvers developed by Pauli Virtanen[2], based on earlier work[3–5]. The

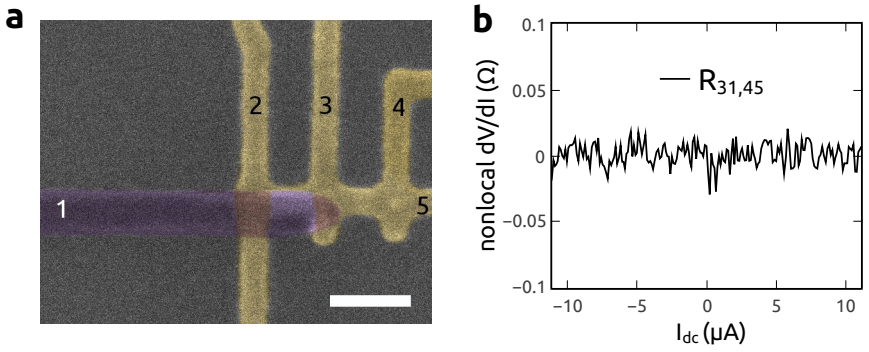

FIG. 2: **(a)** Scanning electron micrograph of control sample similar to that of Fig. 1 of the main text, but with no second superconductor. Size bar is 200 nm. **(b)** Nonlocal resistance measurement on the sample of **a**, showing that there is no nonlocal signal in the absence of the second superconductor.

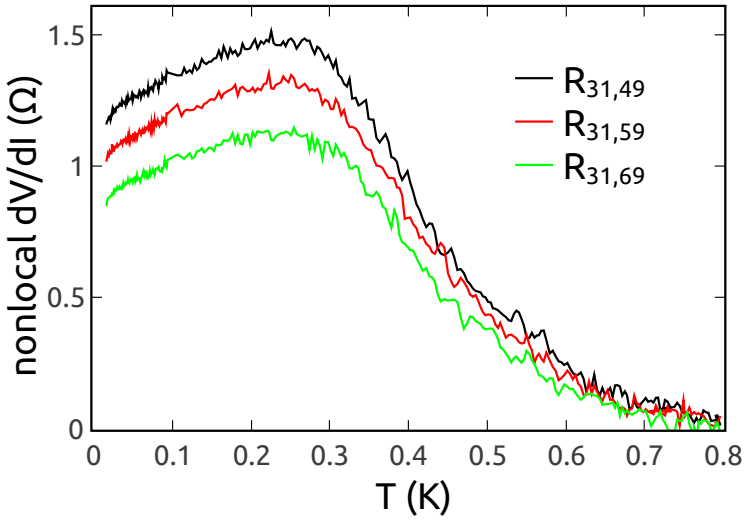

FIG. 3: **(a)** Temperature dependence of the zero bias nonlocal resistance of the sample of Fig. 1 of the main text.

starting point for the simulations is the equation for the total current

$$\mathbf{j}(\mathbf{R},T) = eN_0D\int dE[M_{33}(\partial_{\mathbf{R}}h_T) + Qh_L + M_{03}(\partial_{\mathbf{R}}h_L)]. \quad (1)$$

Here N_0 is the electronic density of states at the Fermi energy, D is the electronic diffusion coefficient, h_T and h_L are the tranverse and longitudinal quasiparticle distribution functions,

which in equilibrium at energy E in reservoirs at a potential V have the form

$$h_{L,T} = \frac{1}{2}\left[\tanh\left(\frac{E+eV}{2k_BT}\right) \pm \left(\frac{E-eV}{2k_BT}\right)\right], \tag{2}$$

the spectral supercurrent Q is given by

$$Q = \Re\left(2N^2[\gamma\nabla\tilde{\gamma} - \tilde{\gamma}\nabla\gamma]\right) \tag{3}$$

and the dimensionless diffusion coefficients M by

$$M_{33} = |N|^2(|\gamma|^2+1)(|\tilde{\gamma}|^2+1) \tag{4}$$

and

$$M_{03} = |N|^2(|\tilde{\gamma}|^2 - |\gamma|^2), \tag{5}$$

where $N = (1+\gamma\tilde{\gamma})^{-1}$. γ, $\tilde{\gamma}$ are the Riccati parametrization parameters that satisfy the coupled equations

$$D\nabla^2\gamma - 2N\tilde{\gamma}|\nabla\gamma|^2 + 2iE\gamma = 0, \tag{6}$$

and

$$D\nabla^2\tilde{\gamma} - 2N\gamma|\nabla\tilde{\gamma}|^2 + 2iE\tilde{\gamma} = 0 \tag{7}$$

in the normal metal wires. The boundary conditions for the differential equations are that γ and $\tilde{\gamma}$ are zero at a normal reservoir, while on a superconducting reservoir

$$\gamma^R = -\frac{\Delta}{E+i\sqrt{|\Delta|^2-(E+i\delta)^2}}, \tilde{\gamma}^R = \frac{\Delta^*}{E+i\sqrt{|\Delta|^2-(E+i\delta)^2}}, \tag{8}$$

where $\Delta = |\Delta|e^{i\phi}$ is the complex order parameter in the superconducting reservoir, ϕ being the phase of the superconductor.

The first term on the RHS in Eqn (1) is the quasiparticle current, the second term is the supercurrent, and the third term corresponds to conversion of quasiparticle to supercurrent, and is typically negligible in a normal metal. At the nodes, the Riccati parameters are continuous, and their derivatives sum to zero. The spectral charge and energy currents also sum to zero along a node, and are conserved in a normal wire.

To calculate the differential resistance as a function of the current, we use the sample geometry in Fig. 3a of the main text. A voltage V is applied to the normal contact N_1 with the superconducting reservoirs S_1 and S_2 being at zero potential, and the resulting current

I_{qp} flowing from N_1 is calculated under the boundary condition that no current flows into contacts N_2, N_3 and S_2. In order to satisfy these boundary conditions, the voltages V_{nl1} and V_{nl2} on the normal contacts N_2 and N_3 and the phase difference ϕ between the two superconducting contacts S_1 and S_2 are adjusted in an iterative loop. As I_{qp} increases, a quasiparticle current I_{qp2} flows into S_2, which is counterbalanced by a supercurrent I_S that flows from S_2 to S_1. As I_S approaches the critical current, the simulations have greater difficulty converging, and we have shown in the figures in the main text only that range of I_{qp} over which the boundary conditions are satisfied. For the plot, the nonlocal differential resistances dV_{nl1}/dI_{qp} and dV_{nl2}/dI_{qp} are calculated numerically. Taking the length of the wire between the superconducting reservoirs to be L, the nonlocal resistances shown in the simulations of Fig. 3b of the main text correspond to the positions of the normal leads in the actual sample (Fig. 1a of the main text), with the length of each normal reservoir from the proximity coupled normal wire being 0.75 L. We have also performed simulations with different values of this length, and this value most closely resembles the shape of the experimental curve. The temperature of the simulations correspond to 20 mK.

For the temperature dependence, a similar simulation was done, but only a small voltage $\pm V$ was applied to N_1, and the resulting values used to calculate the differential resistances as a function of temperature.

---

[1] Cadden-Zimansky, P. & Chandrasekhar, V. Nonlocal correlations in normal-metal superconducting systems. *Phys. Rev. Lett.* **97**, 237003 (2006).

[2] Virtanen, P. http://ltl.tkk.fi/∼theory/usadel1.html

[3] Belzig, W., Wilhelm, F. K., Bruder, C., Schn, G. & Zaikin, A. D. Quasiclassical Green's function approach to mesoscopic superconductivity. *Superlattices Microstruct* **25**, 1251 (1999)

[4] Chandrasekhar, V. An introduction to the quasiclassical theory of superconductivity for diffusive proximity-coupled systems. In The *Physics of Superconductors*, vol II, eds. Bennemann and Ketterson, Springer-Verlag, (2004)

[5] Virtanen, P. & Heikkil. T. T. Thermoelectric effects in superconducting proximity structures. *Appl. Phys. A* **89**, 625 (2007)